Acta Crystallographica Section F
Structural Biology and Crystallization Communications
ISSN 1744-3091

Crystallization and preliminary X-ray analysis of the chemokine-binding protein from orf virus (*Poxviridae*)

Rafael Miguez Couñago,[a] Stephen B. Fleming,[b] Andrew A. Mercer[b] and Kurt L. Krause[a]*

[a]Department of Biochemistry, University of Otago, New Zealand, and [b]Department of Microbiology and Immunology, University of Otago, New Zealand

Correspondence e-mail: kurt.krause@otago.ac.nz

Received 1 April 2010
Accepted 17 May 2010

The parapoxvirus orf virus (ORFV) encodes a chemokine-binding protein (CBP) that functions to downregulate the host's immune response at the site of infection by blocking the chemokine-induced recruitment of immune cells. In order to shed light on the structural determinants of CBP–chemokine binding, ORFV CBP was crystallized as part of an ongoing structure–function study on this protein. ORFV CBP crystals were obtained by the sitting-drop vapour-diffusion technique using ammonium citrate as a precipitant. The crystal quality was greatly improved through the addition of small-molecule additives to the crystallization mother liquor. ORFV CBP crystals diffracted X-rays to 2.50 Å resolution and belonged to the hexagonal space group $P6_122$ or its enantiomorph $P6_522$, with unit-cell parameters $a = b = 75.62$, $c = 282.49$ Å, $\alpha = 90$, $\beta = 90$, $\gamma = 120^\circ$.

1. Introduction

Chemokines are small (8–14 kDa) secreted proteins that regulate inflammation-induced leukocyte recruitment to the sites of infection as well as the homeostatic migration of leukocytes through lymphoid organs (Baggiolini, 1998). Members of the chemokine superfamily can be classified into four subfamilies (CC, C*X*C, CX_3C or C, where *X* is any residue) based on the arrangement of the highly conserved cysteine residues that are involved in disulfide-bond formation at the N-terminus (Rollins, 1997). Chemokines function as attractants to leukocytes, signalling through G-protein-coupled receptors (GPCRs) on the cell surface (Murphy, 1994). The association of chemokines with glycosaminoglycans (GAGs) in the extracellular matrix facilitates the retention of these molecules and the formation of a concentration gradient radiating from chemokine-producing cells (Yu *et al.*, 2005; Proudfoot *et al.*, 2003; Hoogewerf *et al.*, 1997; Middleton *et al.*, 1997). Secretion of pro-inflammatory chemokines is upregulated during viral infections (Baggiolini, 1998) and in some autoimmune diseases (Rotondi *et al.*, 2007). Despite the poor sequence identity observed for members of the chemokine superfamily, they share a similar tertiary structure (an N-terminal extended loop and a C-terminal Greek-key motif formed by a three-stranded β-sheet) and bind to their cognate receptors with picomolar affinities (Fernandez & Lolis, 2002; Lau *et al.*, 2004).

Members of the chordopoxvirus subfamily encode a set of secreted proteins called chemokine-binding proteins (CBPs). They disrupt chemokine signalling and prevent leukocyte recruitment to the site of infection (Smith *et al.*, 1997; Lateef *et al.*, 2009; Seet *et al.*, 2003; Alcami *et al.*, 1998; Graham *et al.*, 1997). Furthermore, a subset of poxviral proteins called vCCIs has been described which bind chemokines from the CC subfamily with picomolar affinity (Smith *et al.*, 1997; Lateef *et al.*, 2009). To date, four structures of vCCIs are available: the vCCIs from rabbitpox virus (PDB code 2ffk; Zhang *et al.*, 2006) and cowpox virus (PDB code 1cq3; Carfi *et al.*, 1999), the EVM1 protein from ectromelia virus (PDB code 2grk; Arnold & Fremont, 2006) and the A41 protein from vaccinia virus (PDB code 2vga; Bahar *et al.*, 2008). EVM1 and the first two vCCI proteins share between 80 and 85% sequence identity. On the other hand, the vaccinia virus A41 protein is only 22% identical in sequence to the

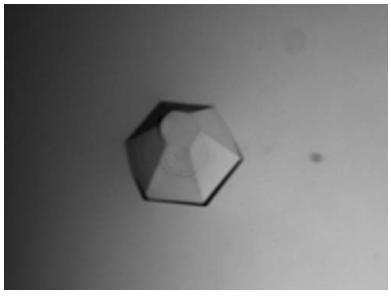

ectromelia virus EVM1 protein. All these viral chemokine-binding proteins share a conserved β-sandwich topology with no resemblance to GPCRs (Arnold & Fremont, 2006; Bahar *et al.*, 2008; Carfi *et al.*, 1999; Zhang *et al.*, 2006). Structural studies of vCCIs in complex with host CC chemokines (Carfi *et al.*, 1999; Zhang *et al.*, 2006) and mutagenesis experiments (Beck *et al.*, 2001; Arnold & Fremont, 2006) have shown that the ability of vCCIs to bind different host chemokines arises from the presence of a patch of charged residues on β-sheet II of the viral protein. These studies suggest a general mechanism of action for vCCIs that involves binding of the targeted CC chemokine at the site through which the chemokine would normally interact with its host-cell receptor, thus blocking their ability to deploy effectively during infection or inflammation (Arnold & Fremont, 2006; Bahar *et al.*, 2008; Beck *et al.*, 2001; Carfi *et al.*, 1999; Zhang *et al.*, 2006; Seet *et al.*, 2003).

Orf virus (ORFV) is the prototypical parapoxvirus, but the sequence of its chemokine-binding protein has low identity to other viral chemokine-binding proteins (the highest identity is 18%). Also, its sequence contains only six of the eight cysteine residues that are conserved in other poxvirus chemokine-binding proteins. *In vitro*, ORFV CBP has shown the unusual ability to bind chemokines from two different subfamilies: CC and C (Seet *et al.*, 2003). These results suggest that ORFV CBP does not fit well within the vCCI family and may represent a unique subclass of chemokine-binding protein. Previous work has also shown that ORFV CBP can dampen the inflammatory response in a mouse skin model (Lateef *et al.*, 2009). In order to define how ORFV CBP interacts with chemokines and to elucidate whether it comprises a unique chemokine-binding fold, we are working to determine its three-dimensional structure. Here, we describe the expression, purification and preliminary X-ray analysis of the chemokine-binding protein from ORFV.

2. Materials and methods

2.1. Expression and purification of ORFV CBP

The coding region for the CBP from ORFV strain NZ2 (GenBank ABA00630.1) was amplified from the pAPEX-3 vector (Seet *et al.*, 2003) by PCR using the forward primer 5′-CGC **GAA TTC** GCC ACC ATG AAG GCG GTG TTG TTG CTG-3′ and the reverse primer 5′-GCG **AAG CTT** TCA GTG GTG GTG GTG GTG GTG GGA CTG GAA GTA CAG GTT TTC ATT GCC AGG GTT GAG GTT AAG-3′ (bold nucleotides indicate restriction sites: *Eco*RI on the forward primer and *Hin*dIII on the reverse primer). The ORFV CBP amplicon was introduced into the *Eco*RI/*Hin*dIII sites of plasmid pTT5 (Zhang *et al.*, 2009), a derivative of vector pTT (Durocher *et al.*, 2002). The recombinant DNA construct was introduced into *Escherichia coli* strain DH5α (Bethesda Research Laboratories, 1986) through electroporation (Sambrook & Russell, 2006). Milligram quantities of pTT5/CBP plasmid were isolated from *E. coli* DH5α cells grown on liquid ZYM-505 medium (Studier, 2005) using the Plasmid Mega Kit from Qiagen (Valencia, California, USA). ORFV CBP was produced following transient transfection of suspension-growing HEK293-6E cells with pTT5/CBP following the method developed by Durocher *et al.* (2002). The recombinant protein expressed from HEK293-6E included a C-terminal TEV protease-cleavable His_6 tag (the His_6 and TEV cleavage site were introduced into the ORFV CBP construct through the reverse primer during cloning). Secreted His_6-tagged ORFV CBP was purified from the cell-culture medium 144 h post-transfection by immobilized metal-ion affinity chromatography (IMAC) in the following manner. HEK293-6E cells were removed from the culture medium by centrifugation (5000*g* for 10 min). To the clarified cell medium, sufficient 1.0 *M* Tris–HCl pH 8.0, 50%(*v*/*v*) glycerol, 5.0 *M* NaCl and 1.0 *M* imidazole pH 8.0 was added to achieve a final concentration of 50 m*M* Tris–HCl, 10%(*v*/*v*) glycerol, 150 m*M* NaCl and 30 m*M* imidazole. The conditioned cell medium was concentrated using a stirred cell (model 8400, Amicon) fitted with a regenerated cellulose ultrafiltration membrane (YM10, 76 mm diameter; Millipore, Billerica, Massachusetts, USA) and applied onto a 5 ml HisTrap FF Crude column (GE Healthcare) pre-equilibrated with equilibration buffer [50 m*M* Tris–HCl pH 8.0, 10%(*v*/*v*) glycerol, 150 m*M* NaCl and 30 m*M* imidazole]. The column was washed with 20 column volumes of equilibration buffer. His-tagged ORFV CBP was eluted with five column volumes of 130 m*M* imidazole in equilibration buffer. Fractions containing ORFV CBP were dialyzed overnight at 277 K against TEV protease reaction buffer (50 m*M* Tris–HCl pH 8.0, 0.5 m*M* EDTA, 1 m*M* DTT). The C-terminal His_6 tag was removed from ORFV CBP by overnight treatment with His_6-tagged TEV protease at 277 K (1:5 molar ratio of protease to ORFV CBP). ORFV CBP without the His_6 tag was purified from the TEV reaction mixture using the same IMAC strategy as described above. Column-flowthrough fractions containing ORFV CBP were pooled together and concentrated using Amicon ultracentrifugal devices (molecular-weight cutoff 10 000 Da; Millipore). ORFV CBP was further purified by size-exclusion chromatography on a Superdex 200 HiLoad 26/60 column (GE Healthcare) pre-equilibrated with 50 m*M* Tris–HCl pH 8.0, 150 m*M* NaCl and 1 m*M* DTT. Fractions containing ORFV CBP were pooled together and dialysed overnight into crystallization buffer (25 m*M* HEPES pH 7.0, 1.0 m*M* DTT). ORFV CBP was concentrated to $\sim$34 mg ml^{-1} in crystallization buffer using Amicon ultracentrifugal devices (molecular-weight cutoff 10 000 Da; Millipore). Aliquots (50–100 µl) of ORFV CBP were flash-frozen in liquid nitrogen and stored at 193 K. The protein concentration was estimated using the Coomassie Plus (Bradford) Protein Assay (Thermo Scientific). Recombinant ORFV CBP contains the following extra C-terminal residues from the TEV recognition sequence: ENLYFQ.

2.2. Dynamic light-scattering analysis

Quasi-elastic light scattering of purified ORFV CBP (20 µl; 1 mg ml^{-1} in crystallization buffer at 289 K) was performed on a DynaPro 99E instrument and analysed using *DYNAMICS* software (Protein Solutions). All samples were passed through a 0.02 µm Anotop 10 filter (Whatman, Maidstone, England) prior to DLS analysis.

2.3. Mass-spectrometric analysis

Mass-spectrometric analyses of ORFV CBP samples were performed by the Centre of Protein Research at the University of Otago. For intact mass determination, samples were analysed on a 4800 MALDI tandem time-of-flight analyzer (MALDI TOF/TOF; Applied Biosystems, Masschusetts, USA). For peptide identification, samples were separated using SDS–PAGE and the bands of interest were excised from the gel and treated with trypsin. The resulting peptides were analysed on a 4800 MALDI TOF/TOF (Applied Biosystems, Massachusetts, USA). The 15–20 strongest precursor ions of each sample spot were selected for MS/MS collision-induced dissociation analysis. MS/MS data were searched against the UniProt/SWISS-PROT amino-acid sequence database using the *Mascot* search engine (http://www.matrixscience.com).

2.4. Crystallization and X-ray data collection

Initial screenings for crystallization conditions were performed at 289 and 277 K using the hanging-drop and sitting-drop vapour-diffusion techniques in 96-well microplates (Sarstedt Australia Pty Ltd) and employed commercially available crystallization screens (Index HT, PEG/Ion HT and Crystal Screen HT from Hampton Research, Aliso Viejo, California, USA). Crystallization trays were set up using a Mosquito robot (TTP LabTech, Royston, Hertfordshire, England). A 0.2 µl droplet of 34 mg ml^{-1} ORFV CBP in 25 m*M* HEPES pH 7.0, 1.0 m*M* DTT was mixed with an equal volume of a reservoir solution. The droplet was allowed to equilibrate against 100 µl reservoir solution.

Hits from initial crystallization screens were further optimized by varying the protein and precipitant concentrations and by the addition of small molecules. Crystallization screens for small-molecule additives were performed in 96-well plates as described above using Silver Bullets from Hampton Research (McPherson & Cudney, 2006). For these screens, the crystallization droplet consisted of 300 nl reservoir solution, 300 nl protein solution and 200 nl Silver Bullets. Further screens and growth of large crystals for data collection were performed in 24-well Linbro plates (Hampton Research, Aliso Viejo, California, USA) using the hanging-drop vapour-diffusion technique. Crystallization droplets (6 µl total volume; 3 µl ORFV CBP at 12 mg ml^{-1} plus 3.0 µl of a solution containing the desired concentration of additive dissolved in 1.8 *M* ammonium citrate tribasic) were placed onto siliconized cover slides (Hampton Research, Aliso Viejo, California, USA) and equilibrated against 1.0 ml reservoir solution. ORFV CBP crystals could be observed after 5–7 d at 289 K.

Crystals utilized for X-ray diffraction analysis were mounted in nylon loops (Hampton Research, Aliso Viejo, California, USA) and flash-cooled directly in a nitrogen cryostream at 100 K (Garman & Schneider, 1997); the same temperature was used for X-ray data collection. Alternatively, crystals were plunged directly into a liquid-nitrogen bath or into a 2-methylbutane (Sigma-Aldrich) bath cooled to 100 K. For the analysis of X-ray diffraction quality at room temperature, crystals were mounted using MicroMounts and covered with MicroRT X-ray capillaries containing 10–20 µl reservoir solution (MiTeGen, Ithaca, New York, USA). The X-ray diffraction quality of these crystals was assessed following two short exposures taken 90° apart.

X-ray diffraction images for ORFV CBP crystals were collected on a Micromax-007 HF rotating-anode X-ray generator equipped with a copper anode, Hi-Res optics and an R-AXIS IV++ image-plate detector (Rikagu). Images were recorded using a frame width of 0.5°, an exposure time of 90–300 s and a crystal-to-detector distance of 260 mm.

Images were processed, scaled and merged using the programs within the *CrystalClear* software package (Pflugrath, 1999). Further data analysis, including a survey of systematic absences and calculation of the Matthews coefficient, was conducted using software within the *CCP*4 suite (Collaborative Computational Project, Number 4, 1994).

3. Results and discussion

The full-length CBP from ORFV strain NZ2 was expressed in HEK293-6E cells transiently transfected with plasmid pTT5/CBP. Upon expression, ORFV CBP accumulated in the extracellular medium, as previously reported (Seet *et al.*, 2003).

ORFV CBP could be purified to homogeneity from the cell-culture medium. In the last purification step, involving size-exclusion chromatography, ORFV CBP eluted as a single peak (Fig. 1*a*), but SDS–PAGE analysis of the purified protein showed the presence of multiple bands (Fig. 1*b*). Mass-spectrometric analysis of these bands identified them all as ORFV CBP (data not shown). The molecular weights of the bands corresponded roughly to what would be expected for a monomer, a dimer and a higher oligomer, either a trimer or a tetramer, but all were somewhat higher than expected.

The molecular weight of an intact CBP monomer, as determined by mass spectrometry (MALDI TOF/TOF), is 36.7 kDa (data not shown). This figure is larger than that calculated from the primary sequence (31.3 kDa), but close to what is seen on the SDS–PAGE gel. Knowing that glycosylation is a common event for viral proteins produced in eukaryotic hosts and that ORFV CBP contains several putative glycosylation sites, we attempted to resolve the discrepancy between the observed and predicted molecular mass of the ORFV CBP monomer by the treatment of purified protein with deglycosylation enzymes. This treatment reduced the apparent molecular weight of the protein to a value that was much closer to that calculated from the primary sequence (data not shown). The

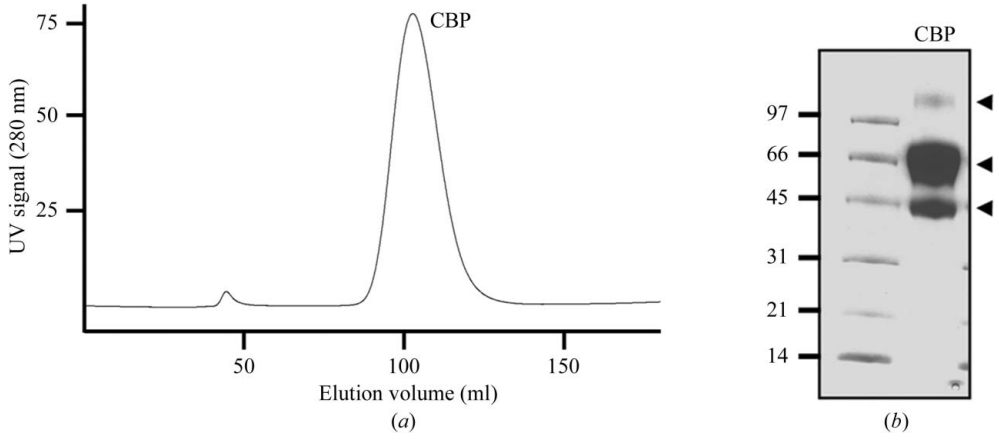

Figure 1
Analysis of purified ORFV CBP by size-exclusion chromatography (*a*) and SDS–PAGE (*b*). (*a*) Chromatogram from size-exclusion chromatography of approximately 4 mg IMAC-purified TEV-treated ORFV CBP on a Superdex 200 HiLoad 26/60 column; the UV signal is in arbitrary absorbance units. (*b*) ∼10 µg of the peak fraction from (*a*) (labelled CBP) was separated by electrophoresis on a denaturing 4–20% polyacrylamide gradient gel. SDS–PAGE was performed under reducing conditions. The numbers on the left indicate the molecular weight in kDa of the marker proteins (left lane). All three protein bands visible in the CBP lane (arrowheads) were identified as ORFV CBP by mass spectrometry following tryptic digestion.

discrepancy in molecular weight that we observed is therefore at least in part a consequence of post-translational glycosylation of ORFV CBP by HEK293-6E cells.

The behaviour of ORFV CBP in solution was further characterized using dynamic light scattering (DLS). Analysis of the DLS data revealed a single species in solution with an estimated molecular weight of 75 kDa and a polydispersity of 8.5% (data not shown). Together with the intact mass of an ORFV CBP monomer estimated by mass spectrometry at 36.7 kDa, the DLS data suggest that ORFV CBP is a dimer in solution.

Initial crystallization screens (a total of 576: 288 distinct conditions set up at two temperatures) of purified glycosylated ORFV CBP were performed using 0.2 µl volume drops in 96-well microplates. These screens identified eight conditions in which crystals could be observed. Notably, seven of these initial crystal hits contained 20–25%(*w*/*v*) PEG 3350 as the precipitant. One crystallization hit was observed with 1.80 *M* ammonium citrate tribasic pH 7.0 as the precipitant. The same eight conditions produced crystals at 289 and 277 K. Preliminary X-ray diffraction analysis of these crystals suggested that those grown from the ammonium citrate condition displayed superior diffraction quality (as judged by resolution limit, spot shape and anisotropy) compared with those obtained from the PEG conditions (data not shown). Moreover, large ORFV CBP crystals grown in ammonium citrate were easier to obtain in the higher volume drops that were set up using 24-well plates.

Initial ORFV CBP crystals grown in vapour-diffusion experiments with 1.80 *M* ammonium citrate as the precipitant displayed no sharp edges (Figs. 2*a* and 2*e*) and diffracted X-rays to 3.0 Å resolution (data not shown). The overall morphology and X-ray diffraction quality of these crystals were not affected by using either the sitting-drop or hanging-drop vapour-diffusion approaches. These initial crystals were greatly optimized by the addition of small molecules to the crystallization droplet. It has been suggested that small molecules can stabilize protein conformation, improve protein solubility or facilitate crystal contacts, thus improving crystal quality (McPherson & Cudney, 2006). Addition of a mixture of small peptides (Gly-Phe, Gly-Tyr and Leu-Gly-Gly) dramatically improved the crystal morphology (Figs. 2*b*, 2*c* and 2*d*). More importantly, these crystals displayed higher resolution limits (up to 1.9 Å at room temperature) and less anisotropy than the originally obtained crystals. Addition of L-Arg and glucose also had a positive effect on crystal morphology (Figs. 2*f*–2*i*) and a similar impact on X-ray diffraction quality. In all cases, crystal-quality improvement was directly related to how much additive was included in the crystallization. Attempts to crystallize deglycosylated ORFV CBP under these optimized conditions have not been successful to date.

Flash-cooling ORFV CBP crystals directly in a gaseous nitrogen stream (set at 100 K) had a negative impact on the diffraction quality of the crystal. Visual inspection of mounted flash-cooled crystals indicated that both the crystal and its surrounding solution remained clear within the cryoloop and no ice rings could be detected on X-ray images. Quick soaks (1–15 s) in varying concentrations of commonly used cryoprotectants did not preserve crystal diffraction quality following flash-cooling. Longer incubations in cryosolutions (30 s to

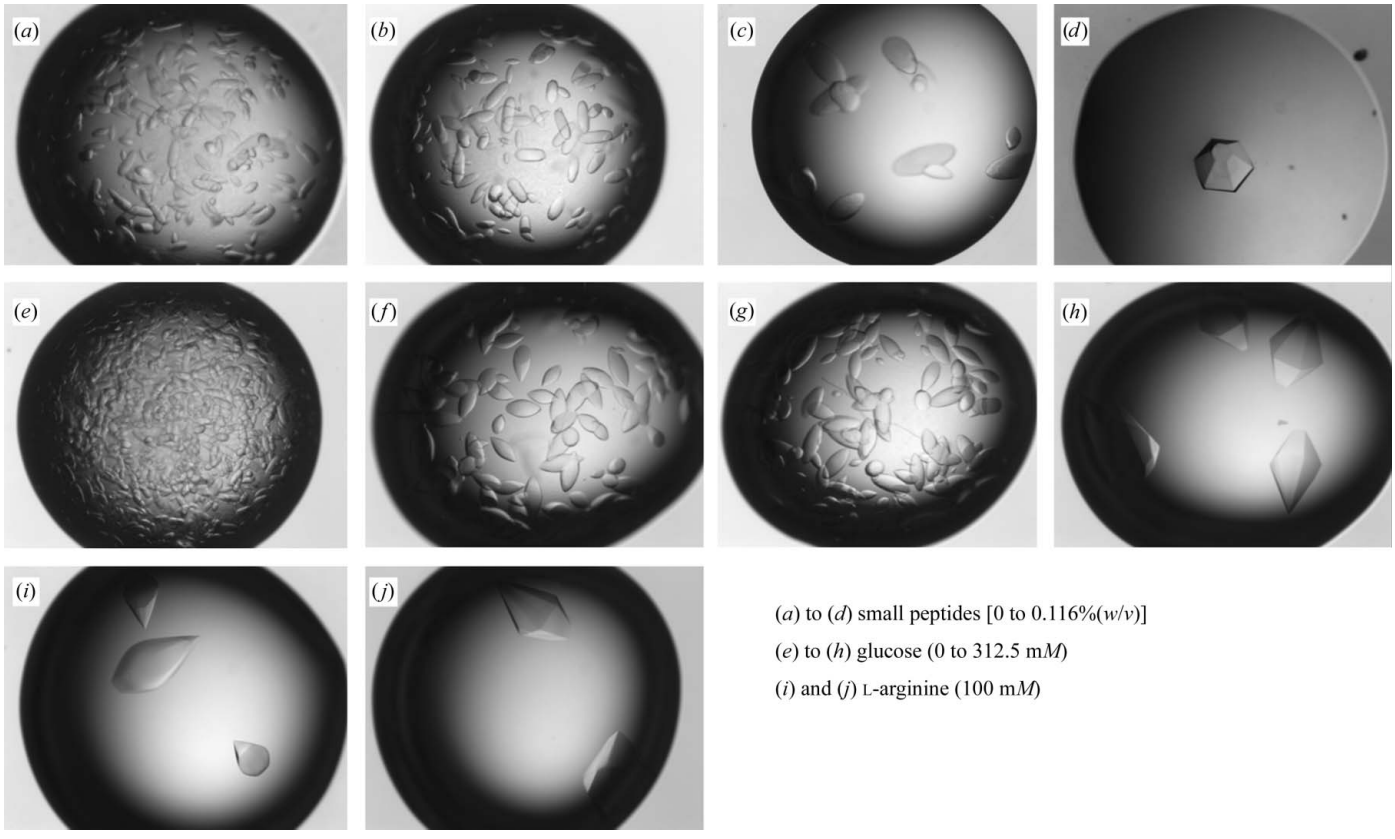

Figure 2
Effect of small-molecule additives on ORFV CBP crystals. Crystals were grown in 1.80 *M* ammonium citrate tribasic pH 7.0 in the presence of no additives (*a*, *e*) or varying concentrations of a small-peptide cocktail containing Gly-Phe, Gly-Tyr and Leu-Gly-Gly (*b*, *c*, *d*), glucose (*f*, *g*, *h*) or a fixed amount (100 m*M*) of L-arginine (*i*, *j*). The protein concentration in (*a*)–(*d*) and that in (*i*) was 10 mg ml^{-1}. The protein concentration in (*e*)–(*h*) and (*j*) was 18 mg ml^{-1}. The concentration of the small-peptide cocktail was 0.033%(*w*/*v*) in (*b*), 0.083%(*w*/*v*) in (*c*) and 0.116%(*w*/*v*) in (*d*). The concentration of glucose was 93.75 m*M* in (*f*), 156.25 m*M* in (*g*) and 312.5 m*M* in (*h*). The crystals in (*a*) have approximate dimensions of 0.2 × 0.1 × 0.1 mm. The crystals in (*d*), (*h*), (*i*) and (*j*) have dimensions of approximately 0.7 × 0.3 × 0.3 mm.

Table 1
Statistics of data collection and processing.

Wavelength (Å)	1.5418
Space group	$P6_122$ or $P6_522$
Unit-cell parameters (Å, °)	$a = b = 75.62$, $c = 282.4$, $\alpha = \beta = 90$, $\gamma = 120$
Solvent content (%)	61.30
Resolution range (Å)	59.41–2.50 (2.59–2.50)
No. of reflections	154029 (5048)
Unique reflections	16826 (1265)
Redundancy	9.09 (3.98)
Completeness (%)	96.0 (75.0)
$R_{\rm merge}$† (%)	11.8 (58.9)
$I/\sigma(I)$	13.1 (3.8)

† $R_{\rm merge}$ as a percentage is defined as $\sum_{hkl}\sum_i |I_i(hkl) - \langle I(hkl)\rangle|/\sum_{hkl}\sum_i I_i(hkl) \times 100$.

minutes) generally induced cracks in the crystals and led to poor X-ray diffraction. Attempts to sequentially add cryoprotectant to the crystallization drop also led to crystal damage.

Replacing the salt within crystals by PEG has occasionally been shown to be a valid strategy to preserve diffraction quality following flash-cooling (Ray *et al.*, 1991, 1997). Unfortunately, we could not find conditions that allowed ORFV CBP crystals to be transferred from 1.8 *M* ammonium citrate to PEG without damaging the crystals. As an alternative strategy for flash-cooling crystals, we tried plunging crystals directly into liquid-nitrogen baths or into cryocooled 2-methylbutane baths (Garman & Schneider, 1997). Unfortunately, these methods did not improve the X-ray diffraction quality of flash-cooled crystals when compared with the use of a cryostream. Flash-reannealing has also proven to be helpful in some instances in reducing cryocooling-associated degradation of diffraction (Yeh & Hol, 1998). We have determined that for some crystals of CBP flash-annealing does reduce the diffraction anisotropy introduced by the flash-cooling process, but it does not restore the X-ray diffraction to the resolution limits observed for ORFV CBP crystals at room temperature.

Preliminary X-ray diffraction data (200° wedge, 0.5° oscillation angle; Table 1) were collected from a flash-cooled ORFV CBP crystal (0.5 × 0.3 × 0.3 mm) grown in 1.8 *M* ammonium citrate tribasic pH 7.0 in the presence of 100 m*M* L-Arg without the addition of cryoprotectants. Analysis of the diffraction data using *POINTLESS* (Collaborative Computational Project, Number 4, 1994) identified a hexagonal lattice and indicated that systematic absences were identified along c^* (00l) and conformed to the $l = 6n$ rule. Taken together with additional symmetry along a^* and b^*, these results suggest that the most likely space group for the ORFV CBP crystals is the hexagonal space group $P6_122$ or its enantiomorph $P6_522$. The unit-cell parameters for the ORFV CBP crystals are $a = b = 75.62$, $c = 282.49$ Å, $\alpha = \beta = 90$, $\gamma = 120°$. ORFV CBP crystals have a Matthews coefficient of 3.18 Å^3 Da^{-1}, corresponding to a single protein molecule per asymmetric unit and a solvent content of 61.30% (Matthews, 1968).

Attempts to solve the ORFV CBP structure by molecular replacement using the atomic coordinates of other poxviral CBPs as search models have thus far failed. In general, the sequence identity between ORFV CBP and other poxviral CBPs ranges from 16 to 18%. Therefore, the most likely reason for the failure of molecular replacement is the low structural similarity between the CBP from ORFV and the CBP proteins produced by other poxviruses. We are currently exploring a solution to the phase problem based on the use of heavy-atom derivatives.

We thank Catherine McCaughan and Michele Krause for maintaining our tissue-culture facilities, the assistance of the Centre for Protein Research, University of Otago and the financial support from the Health Research Council of New Zealand, the New Zealand Synchrotron Group Limited, the Otago Medical Research Foundation, the Royal Society of New Zealand, National Institutes of Health, the Welch Foundation, the University of Otago and the Australian Synchrotron.

References

Alcami, A., Symons, J. A., Collins, P. D., Williams, T. J. & Smith, G. L. (1998). *J. Immunol.* **160**, 624–633.
Arnold, P. L. & Fremont, D. H. (2006). *J. Virol.* **80**, 7439–7449.
Baggiolini, M. (1998). *Nature (London)*, **392**, 565–568.
Bahar, M. W., Kenyon, J. C., Putz, M. M., Abrescia, N. G., Pease, J. E., Wise, E. L., Stuart, D. I., Smith, G. L. & Grimes, J. M. (2008). *PLoS Pathog.* **4**, e5.
Beck, C. G., Studer, C., Zuber, J.-F., Demange, B. J., Manning, U. & Urfer, R. (2001). *J. Biol. Chem.* **276**, 43270–43276.
Bethesda Research Laboratories (1986). *Bethesda Res. Lab. Focus*, **8**, 9–12.
Carfi, A., Smith, C. A., Smolak, P. J., McGrew, J. & Wiley, D. C. (1999). *Proc. Natl Acad. Sci. USA*, **96**, 12379–12383.
Collaborative Computational Project, Number 4 (1994). *Acta Cryst.* D**50**, 760–763.
Durocher, Y., Perret, S. & Kamen, A. (2002). *Nucleic Acids Res.* **30**, E9.
Fernandez, E. J. & Lolis, E. (2002). *Annu. Rev. Pharmacol. Toxicol.* **42**, 469–499.
Garman, E. F. & Schneider, T. R. (1997). *J. Appl. Cryst.* **30**, 211–237.
Graham, K. A., Lalani, A. S., Macen, J. L., Ness, T. L., Barry, M., Liu, L.-Y., Lucas, A., Clark-Lewis, I., Moyer, R. W. & McFadden, G. (1997). *Virology*, **229**, 12–24.
Hoogewerf, A. J., Kuschert, G. S., Proudfoot, A. E., Borlat, F., Clark-Lewis, I., Power, C. A. & Wells, T. N. (1997). *Biochemistry*, **36**, 13570–13578.
Lateef, Z., Baird, M. A., Wise, L. M., Mercer, A. A. & Fleming, S. B. (2009). *J. Gen. Virol.* **90**, 1477–1482.
Lau, E. K., Allen, S., Hsu, A. R. & Handel, T. M. (2004). *Adv. Protein Chem.* **68**, 351–391.
Matthews, B. W. (1968). *J. Mol. Biol.* **33**, 491–497.
McPherson, A. & Cudney, B. (2006). *J. Struct. Biol.* **156**, 387–406.
Middleton, J., Neil, S., Wintle, J., Clark-Lewis, I., Moore, H., Lam, C., Auer, M., Hub, E. & Rot, A. (1997). *Cell*, **91**, 385–395.
Murphy, P. M. (1994). *Annu. Rev. Immunol.* **12**, 593–633.
Pflugrath, J. W. (1999). *Acta Cryst.* D**55**, 1718–1725.
Proudfoot, A. E., Handel, T. M., Johnson, Z., Lau, E. K., LiWang, P., Clark-Lewis, I., Borlat, F., Wells, T. N. & Kosco-Vilbois, M. H. (2003). *Proc. Natl Acad. Sci. USA*, **100**, 1885–1890.
Ray, W., Bolin, J., Puvathingal, J., Minor, W., Liu, Y. & Muchmore, S. (1991). *Biochemistry*, **30**, 6866–6875.
Ray, W. J., Baranidharan, S. & Liu, Y. (1997). *Acta Cryst.* D**53**, 385–391.
Rollins, B. J. (1997). *Blood*, **90**, 909–928.
Rotondi, M., Chiovato, L., Romagnani, S., Serio, M. & Romagnani, P. (2007). *Endocr. Rev.* **28**, 492–520.
Sambrook, J. & Russell, D. W. (2006). *Molecular Cloning: A Laboratory Manual*, pp. 60–62. New York: Cold Spring Harbor Laboratory Press.
Seet, B. T., McCaughan, C. A., Handel, T. M., Mercer, A., Brunetti, C., McFadden, G. & Fleming, S. B. (2003). *Proc. Natl Acad. Sci. USA*, **100**, 15137–15142.
Smith, C. A., Smith, T. D., Smolak, P. J., Friend, D., Hagen, H., Gerhart, M., Park, L., Pickup, D. J., Torrance, D., Mohler, K., Schooley, K. & Goodwin, R. G. (1997). *Virology*, **236**, 316–327.
Studier, F. W. (2005). *Protein Expr. Purif.* **41**, 207–234.
Yeh, J. I. & Hol, W. G. J. (1998). *Acta Cryst.* D**54**, 479–480.
Yu, Y., Sweeney, M. D., Saad, O. M., Crown, S. E., Hsu, A. R., Handel, T. M. & Leary, J. A. (2005). *J. Biol. Chem.* **280**, 32200–32208.
Zhang, J., Liu, X., Bell, A., To, R., Baral, T. N., Azizi, A., Li, J., Cass, B. & Durocher, Y. (2009). *Protein Expr. Purif.* **65**, 77–82.
Zhang, L., Derider, M., McCornack, M. A., Jao, S.-C., Isern, N., Ness, T., Moyer, R. & LiWang, P. J. (2006). *Proc. Natl Acad. Sci. USA*, **103**, 13985–13990.